

# Wavefront retrieval of amplified femtosecond beams by second-harmonic generation

Rocío Borrego-Varillas,<sup>1,\*</sup> Carolina Romero,<sup>1</sup> Javier R. Vázquez de Aldana,<sup>1</sup>  
Juan M. Bueno,<sup>2</sup> and Luis Roso<sup>3</sup>

<sup>1</sup>Departamento de Física Aplicada, Universidad de Salamanca, E-37008 Salamanca, Spain

<sup>2</sup>Laboratorio de Óptica, Universidad de Murcia, Campus de Espinardo (CiOyN), E-30071 Murcia, Spain

<sup>3</sup>Centro de Láseres Pulsados, E-37008 Salamanca, Spain

\*[rociobv@usal.es](mailto:rociobv@usal.es)

**Abstract:** We present a new approach for wavefront characterization of near transform-limited intense femtosecond beams using the angular and spectral dependences of the second-harmonic generation conversion efficiency in uniaxial crystals. The method is applied to different aberrated beams and results are compared with the measurements performed with a commercial sensor, finding very good agreement. The phase retrieval dependence with different parameters (e.g. crystal thickness) is discussed. Successful application to sharpen intensity profiles is also demonstrated.

©2011 Optical Society of America

**OCIS codes:** (010.7350) Wave-front sensing; (320.7110) Ultrafast nonlinear optics; (120.5050) Phase measurement; (320.7100) Ultrafast measurements; (190.4410) Nonlinear optics, parametric processes.

---

## References and links

1. D. Strickland and G. Mourou, "Compression of amplified chirped optical pulses," *Opt. Commun.* **56**(3), 219–221 (1985).
2. T. Brabec and F. Krausz, "Intense few-cycle laser fields: Frontiers of nonlinear optics," *Rev. Mod. Phys.* **72**(2), 545–591 (2000).
3. S.-W. Bahk, P. Rousseau, T. A. Planchon, V. Chvykov, G. Kalintchenko, A. Maksimchuk, G. A. Mourou, and V. Yanovsky, "Generation and characterization of the highest laser intensities ( $10^{22}$  W/cm<sup>2</sup>)," *Opt. Lett.* **29**(24), 2837–2839 (2004).
4. S. Ranc, G. Chériaux, S. Ferré, J.-P. Rousseau, and J.-P. Chambaret, "Importance of spatial quality of intense femtosecond pulses," *Appl. Phys. B* **70**, 181–187 (2000).
5. J. M. Bueno, B. Vohnsen, L. Roso, and P. Artal, "Temporal wavefront stability of an ultrafast high-power laser beam," *Appl. Opt.* **48**(4), 770–777 (2009).
6. C. P. Hauri, J. Biegert, U. Keller, B. Schaefer, K. Mann, and G. Marowski, "Validity of wave-front reconstruction and propagation of ultrabroadband pulses measured with a Hartmann-Shack sensor," *Opt. Lett.* **30**(12), 1563–1565 (2005).
7. J. Primot, "Three-wave lateral shearing interferometer," *Appl. Opt.* **32**(31), 6242–6249 (1993).
8. S. Velghe, J. Primot, N. Guérineau, M. Cohen, and B. Wattellier, "Wave-front reconstruction from multidirectional phase derivatives generated by multilateral shearing interferometers," *Opt. Lett.* **30**(3), 245–247 (2005).
9. J.-C. Chanteloup, F. Druon, M. Nantel, A. Maksimchuk, and G. Mourou, "Single-shot wave-front measurements of high-intensity ultrashort laser pulses with a three-wave interferometer," *Opt. Lett.* **23**(8), 621–623 (1998).
10. R. Grunwald, U. Neumann, U. Griebner, K. Reimann, G. Steinmeyer, and V. Kebbel, "Ultrashort-pulse wave-front autocorrelation," *Opt. Lett.* **28**(23), 2399–2401 (2003).
11. E. Rubino, D. Faccio, L. Tartara, P. K. Bates, O. Chalus, M. Clerici, F. Bonaretti, J. Biegert, and P. Di Trapani, "Spatiotemporal amplitude and phase retrieval of space-time coupled ultrashort pulses using the Shackled-FROG technique," *Opt. Lett.* **34**(24), 3854–3856 (2009).
12. P. R. Bowlan and R. Trebino, "Using Phase Retrieval to Obtain the Complete Spatio-Temporal Intensity and Phase of Ultrashort Pulses," in *Signal Recovery and Synthesis*, OSA Technical Digest (CD) (Optical Society of America, 2009), paper SWA6.
13. A. Marcinkevičius, R. Tommasini, G. D. Tsakiris, K. J. Witte, E. Gaižauskas, and U. Teubner, "Frequency doubling of multi-terawatt femtosecond pulses," *Appl. Phys. B* **79**(5), 547–554 (2004).
14. J. Hou, Y. Zhang, W. Jiang, and N. Ling, "Second-harmonic generation of beams with aberrations," *J. Opt. Soc. Am. B* **19**(6), 1380–1390 (2002).
15. R. W. Boyd, *Nonlinear Optics* (Academic Press, 2008).
16. V. G. Dmitriev, G. G. Guryadzan, and D. N. Nikogosyan, *Handbook of nonlinear optical crystals* (Springer, 1999).
17. J.-C. Diels and W. Rudolph, *Ultrashort laser pulse phenomena* (Academic Press, 1996), Chap. 3.

18. E. Sidick, A. Knoesen, and A. Dienes, "Ultrashort pulse second harmonic generation I: transformed limited fundamental pulses," *J. Opt. Soc. Am. B* **12**(9), 1704–1712 (1995).
19. J.-Y. Zhang, J. Y. Huang, H. Wang, K. S. Wong, and G. K. Wong, "Second harmonic generation from regeneratively amplified femtosecond laser pulses in BBO and LBO crystals," *J. Opt. Soc. Am. B* **15**(1), 200–209 (1998).
20. E. Sidick, A. Dienes, and A. Knoesen, "Ultrashort pulse second harmonic generation II: non-transformed limited fundamental pulses," *J. Opt. Soc. Am. B* **12**(9), 1713–1722 (1995).
21. R. DeSalvo, D. J. Hagan, M. Sheik-Bahae, G. Stegeman, E. W. Van Stryland, and H. Vanherzeele, "Self-focusing and self-defocusing by cascaded second-order effects in KTP," *Opt. Lett.* **17**(1), 28–30 (1992).
22. J. P. Caumes, L. Videau, C. Rouyer, and E. Freysz, "Direct measurement of wave-front distortion induced during second-harmonic generation: application to breakup-integral compensation," *Opt. Lett.* **29**(8), 899–901 (2004).
23. P. M. Prieto, F. Vargas-Martín, S. Goelz, and P. Artal, "Analysis of the performance of the Hartmann-Shack sensor in the human eye," *J. Opt. Soc. Am. A* **17**(8), 1388–1398 (2000).
24. G. Mínguez-Vega, C. Romero, O. Mendoza-Yero, J. R. Vázquez de Aldana, R. Borrego-Varillas, C. Méndez, P. Andrés, J. Lancis, V. Climent, and L. Roso, "Wavelength tuning of femtosecond pulses generated in nonlinear crystals by using diffractive lenses," *Opt. Lett.* **35**(21), 3694–3696 (2010).
25. C. Romero, Universidad de Salamanca, Pl. de la Merced s/n., E-37008 Spain, and associates are preparing a manuscript to be called "Second harmonic generation of femtosecond pulses focused on BBO with a diffractive lens."
26. C. Romero, R. Borrego-Varillas, A. Camino, G. Mínguez-Vega, O. Mendoza-Yero, J. Hernández-Toro, and J. R. Vázquez de Aldana, "Diffractive optics for spectral control of the supercontinuum generated in sapphire with femtosecond pulses," *Opt. Express* **19**(6), 4977–4984 (2011).
27. H.-M. Heuck, P. Neumayer, T. Kühl, and U. Wittrock, "Chromatic aberration in petawatt-class lasers," *Appl. Phys. B* **84**(3), 421–428 (2006).

## 1. Introduction

Gigawatt and terawatt femtosecond lasers based on CPA technology [1], able to produce high peak intensities, are routinely used in high-field physics [2]. To focus these pulses near to diffraction limit [3], a good beam quality is required [4]. However, wavefront aberrations due to thermal effects, cavity misalignment [5], and crystal inhomogeneities can degrade considerably the quality of the focal spot. In this sense, both an accurate characterization and appropriate control of the spatial phase would be desirable. The wavefront measurement of these pulses meets, however, some difficulties due to the broad spectrum and the high intensity.

Different methods have been used so far for this purpose. Hauri et al. demonstrated the validity of the Hartmann-Shack (H-S) sensor to measure the phase of this kind of laser systems [6]. Wavefront sensors based on multi-wave lateral shearing interferometry have also been widely used in this field [7–9]. Their main advantages are the achromaticity and a high dynamic range. In particular, in the work presented in [9], Chanteloup et al. measured for the first time using this technique the wavefront of a high-intensity femtosecond laser carrying a strong  $B$  integral.

More recently, a remarkable effort has been made to fully characterize (both in temporal and spatial domains) these pulses, resulting on new techniques to measure, besides the temporal structure, the wavefront [10–12]. In [10], Grunwald et al. demonstrated simultaneous spatial and angular resolution in pulse characterization by use of a combination of a H-S sensor and autocorrelation. In the approach presented in [11], a grating images the beam into a H-S sensor, what allows to retrieve the wavefront for each wavelength. This is combined with a frequency-resolved-optical-gating (FROG) measurement at a single spatial position, allowing to retrieve the full spatiotemporal structure of pulses. Finally, Bowlan et al. measured the spatio-temporal field of pulses with SEA-TADPOLE and retrieved the spatial phase by using a Gerchberg-Saxton algorithm [12].

In this paper, we demonstrate a technique to retrieve the spatial phase (or alternatively the wavefront) of intense short laser pulses through second-harmonic generation (SHG) in non-linear crystals. To our knowledge, this is the first attempt to measure the wavefront of a laser beam by means of non-linear processes. Our approach takes advantage of the wavefront dependence of such process [13, 14], since the efficiency and the spectral properties of the frequency conversion process strongly depend on the angle between the wave vector and the crystal orientation. The technique consists on the measurement of the spectrum of the generated second harmonic (SH) beam along the transversal direction. From this spectral map

it is possible to recover the wavefront of the incident femtosecond beam by means of a retrieval algorithm that is described in the following section.

The paper is organized as follows. In Sect. 2 we present a summary of some theoretical considerations of SHG that will be used throughout the paper as well as the fundamentals of proposed technique. The experimental setup arranged and used in our work is described in Sect. 3. Results of wavefront measurements for different aberrated femtosecond beams are shown in Sect. 4. Measurements are compared to the wavefront retrieved by other techniques and/or to numerical simulations. Sect. 5 is devoted to the conclusions of the work. The goals and limitations of the proposed technique are discussed there.

## 2. Theoretical background

SHG is nowadays a very useful technique to access new wavelength ranges with the available laser sources. An efficient SHG process can be achieved only in media having a large value of the second-order susceptibility and, moreover, certain conditions over the wave vectors of the interacting waves must be fulfilled (phase-matching) [15]. These conditions involve the refractive index equality for the fundamental and the SH beams. One way to efficiently satisfy such a condition is the use of birefringence in anisotropic crystals. In the particular case of a uniaxial crystal (our study will be restricted to these materials), the dependence of the extraordinary index of refraction with the direction of propagation allows to find the directions for which both indices (ordinary and extraordinary) are identical for the fundamental and the SH beam. In this process, the efficient conversion is very sensitive to the propagation direction of the fundamental beam. This angular dependence will be the basis to retrieve the wavefront of a given beam. This wavefront retrieval will be done by measuring the spectrum of the generated SH signal at each point along one axis, as it is discussed below.

Let us suppose a monochromatic plane wave. For the particular case of type-I phase matching in a collinear configuration (both the fundamental and the SH propagating along the same direction  $\theta$ ) and under the approximations of slowly varying envelope and undepleted pump wave, the intensity of the second harmonic beam  $I_{2\omega}$  can be expressed in terms of the intensity of the fundamental wave  $I_\omega$  as [15]:

$$I_{2\omega} = \frac{8d_{\text{eff}}^2 L^2 \pi^2}{n_e(\lambda/2, \theta) n_o^2(\lambda) \varepsilon_0 c} \frac{1}{\lambda^2} PM(\lambda, \theta) I_\omega^2 \quad (1)$$

where  $d_{\text{eff}}$  is the effective non-linear coefficient of the crystal,  $L$  is the crystal length,  $c$  is the speed of light in vacuum,  $\varepsilon_0$  is the vacuum permittivity and  $\theta$  is the angle between the wave vectors of the interacting waves and the optic axis of the crystal.  $\lambda$  is the wavelength of the fundamental wave. The phase mismatch factor  $PM$  is defined as:

$$PM(\lambda, \theta) = \left[ \frac{\sin(\Delta k(\lambda, \theta) L/2)}{\Delta k(\lambda, \theta) L/2} \right]^2 \quad (2)$$

with  $\Delta k(\lambda, \theta)$  being the phase mismatch that, for type-I SHG (ie.,  $oo \rightarrow e$ ) which can be written as:

$$\Delta k(\lambda, \theta) = \frac{4\pi}{\lambda} \left[ n_e(\lambda/2, \theta) - n_o(\lambda) \right] \quad (3)$$

where  $n_o$  and  $n_e$  are the ordinary and extraordinary indices respectively. The dependence of these indices with respect to the wavelength is given by the Sellmeier equations [16].

The strongest dependence of  $I_{2\omega}$  with both the wavelength and the propagation direction comes from the phase mismatch factor  $PM(\lambda, \theta)$ . This function (see Fig. 1a) is peaked at the so-called perfect phase-matching curve  $\Delta k(\lambda, \theta) = 0$  that, from Eq. (3), requires

$n_e(\lambda/2, \theta) = n_o(\lambda)$ . For a given wavelength  $\lambda_0$  there exists a single phase-matching angle  $\theta_0$  satisfying  $\Delta k(\lambda_0, \theta_0) = 0$  that maximizes the SH conversion efficiency.

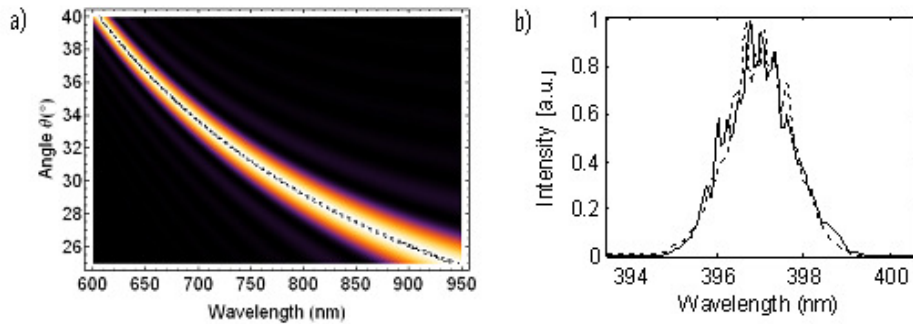


Fig. 1. a) Density plot of the phase mismatch factor  $PM(\lambda, \theta)$  for a BBO crystal of 100  $\mu\text{m}$  thickness. The wavelength values satisfying the perfect phase-matching condition are marked with the dashed line.  $\theta$  is the angle between the wave-vector and the optic axis of the uniaxial crystal. b) Comparison between the measured SH signal (solid line) and the estimation (dashed line) from the fundamental spectrum using Eq. (1) (see details in the text).

In the case of ultra-short pulses, the accurate study of the spectral characteristics of the SH beam requires to solve the wave equations governing the process [17–19]. However, although Eq. (1) was obtained for monochromatic plane waves, it still can be used in a first order approximation to estimate the spectral intensity of the SH signal generated by a femtosecond laser pulse. It is reasonable for moderate intensities (in order to neglect higher-order nonlinear effects), for crystals short enough to neglect dispersion of both the fundamental and SH pulses and for near transform-limited pulses in order to neglect distortions in the SH signal introduced by quadratic or higher order spectral phases [19,20]. In such cases,  $I_o$  is taken as the spectral intensity of the fundamental for each wavelength. Note that this expression (Eq. (1) is a simplified version of the equation given in [17] where only SHG is considered, that is, other frequency mixing processes that could take place among the different wavelengths of the fundamental pulse (i.e. sum-frequency generation) are not accounted for.

The accuracy of using this monochromatic-wave approach has been tested along this work under different experimental conditions. In particular, for a fundamental 120 fs pulse with a central wavelength of 795 nm and a 1 mm thick BBO crystal (typical parameters employed in our study) Fig. 1b compares the measured spectrum of the generated SH pulse with that computed from using Eq. (1). A very good agreement was found that justifies the use of such simple expression in the experimental conditions described here. Neglecting sum-frequency generation is expected to become less reasonable for much shorter pulses. In the framework of this model, we are also neglecting the nonlinear phase distortions induced in non-centrosymmetric crystals due to cascaded processes [21,22], that could play a role in the wavefront retrieval for very high intensities of the fundamental.

On the other hand, in the general case of a non-plane wave, for each point of the transverse plane of the beam,  $I_o$  would be the spectral intensity at this point. In this case  $\theta$  represents the angle between the wave vector (always perpendicular to the wavefront surface) and the optic axis of the crystal at that point. This approximation is meaningful in case of very thin crystals, in which propagation effects (i.e. diffraction) can be neglected. In such conditions, Eq. (1) can be applied to estimate the conversion efficiency for each wavelength of the fundamental beam at any point of its profile by knowing the wavefront. Then, the algorithm now used to retrieve the wavefront is based on the solution of the inverse problem, that is, the spectral intensities of both the fundamental and the SH (and therefore the conversion efficiency for each wavelength) in a set of points along one axis (“scanning” axis)

are known. From this, the wavefront along such axis can be computed by using a retrieval algorithm.

The retrieval algorithm to compute the wavefront in this general case can be summarized as follows. First, the phase mismatch factor  $PM(\lambda, \theta)$  of Eq. (1) is calculated by using the experimental measurements of the spectral intensity of the SH,  $I_{2\omega}$ , and the fundamental,  $I_{\omega}$ . At this point, provided that the main angular dependence of the efficiency comes from the phase mismatch factor, it can be assumed  $n_e(\lambda/2, \theta) \approx n_o(\lambda)$  in the denominator of Eq. (1). Once  $PM(\lambda, \theta)$  is known,  $\Delta k$  is computed from Eq. (2). Finally, equating  $\Delta k$  with Eq. (3) and using Sellmeier expressions for the refractive indices [16], the angle  $\theta$  can be found.  $\theta$  is the angle between the wave vector,  $\mathbf{k}$ , and the optic axis (see caption of Fig. 2a for a detailed description of the geometry).

However, for phase retrieval it is necessary to find the angle  $\alpha$  of the wave vector with respect to the reference axis (z in Fig. 2). If the scanning is made in a plane containing the optic axis (i.e.,  $\varphi = 0^\circ$  according to Fig. 2a), once  $\theta$  is known two possible solutions for  $\alpha$  are possible:

$$\alpha = \alpha_s \pm \theta \quad (4)$$

being  $\alpha_s$  the angle between the optic axis and the propagation axis (in this case, the z-axis).

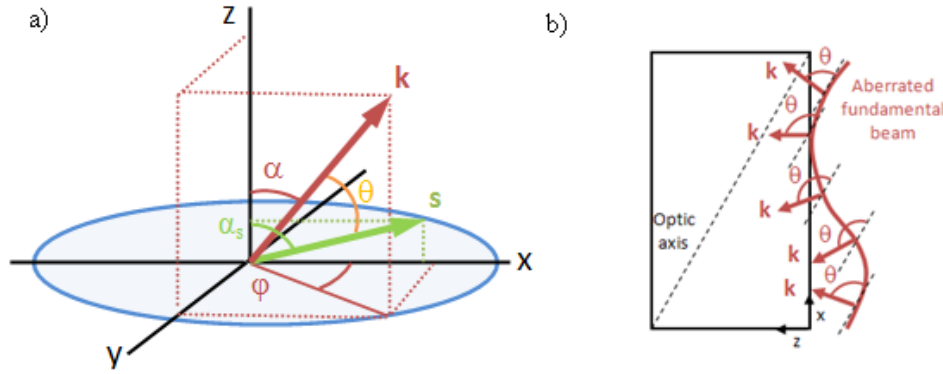


Fig. 2. (a) General diagram for distribution of axes and angles. The beam is assumed to propagate along the z axis.  $\mathbf{k}$  represents the wave vector at a given point of the beam wavefront;  $\mathbf{s}$  is the unitary vector along the optic axis. The section of the beam is showed in blue. (b) Geometry in the particular case where measurements are restricted to the plane containing the optic axis.

In the particular case of using a BBO crystal as non-linear medium, one of these two values for  $\alpha$  can be discarded with the following argument:  $\alpha_s$  will be around  $29.4^\circ$  (phase matching angle for 795 nm), and then the two values for  $\alpha$  are  $29.4^\circ + \theta$  and  $29.4^\circ - \theta$ . However, the critical angle (namely  $\alpha_c$ ) for a wavelength of 795 nm is  $37.0^\circ$ , and it makes the first solution meaningless as it would be only feasible for values of  $\alpha$  between  $29.4^\circ$  and  $37.0^\circ$ , far away from the typical values. Note that this angle corresponds to the one inside the crystal. Thus, it is necessary to take refraction into account through the Snell law:

$$\alpha_0 = \arcsin(n_o(\lambda) \sin(\alpha)) \quad (5)$$

At each scanned point  $x$ , the wavefront is finally reconstructed in terms of  $\lambda$  as:

$$\psi(x) = \psi(x - \Delta x) - \frac{\Delta x \tan(\alpha_0)}{\lambda} \quad (6)$$

where  $\Delta x$  is the increment between two consecutive values of  $x$ .

As an example, Fig. 3 shows a typical sequence of the wavefront retrieval algorithm above described, from the measured spectral map of the SH beam (Fig. 3a) to the final estimation of the wavefront (Fig. 3d). From the spectral map, the phase mismatch factor  $PM(\lambda, \theta)$  is obtained (Fig. 3b), what allows to calculate the extraordinary index. At this point, a Gaussian fitting for the spectrum of the fundamental beam was used to minimize noise in the wavefront retrieval process. Then, Sellmeier equations (for the BBO crystal) are numerically solved in order to compute the distribution of angles  $\theta$  (Fig. 3c). Finally by using Eq. (6), the wavefront (or phase) for a given wavelength is retrieved (Fig. 3d).

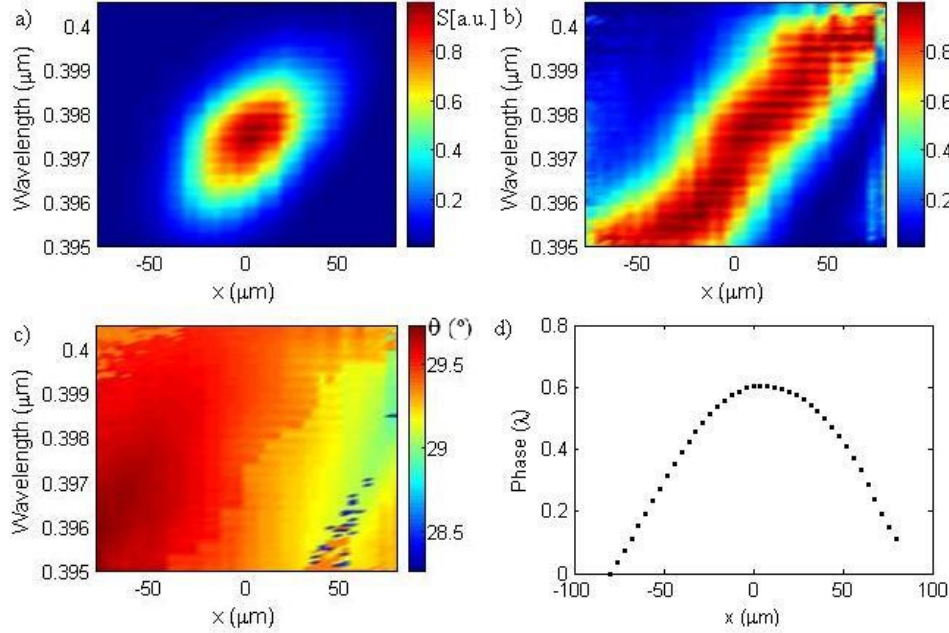


Fig. 3. Example of phase retrieval for a diverging beam using a BBO crystal ( $\alpha_s = 29.4^\circ$ , 500  $\mu\text{m}$  thick): (a) measured spectral map; (b) phase mismatch factor  $PM$ ; (c) map of angles with respect to the optic axis ( $\theta$ , in degrees); (d) retrieved wavefront for the central wavelength (795 nm) of the incident beam (in  $\lambda$  units).

In addition, this algorithm allows exploring the dependence between wavefront and wavelength. This might be useful when using ultra-broadband laser pulses, however under the experimental conditions here reported, no difference between the wavefront recovered for each wavelength was found.

### 3. Experimental setup

The experimental setup used for the aim of this work is shown in Fig. 4. As a laser source a Ti:Sapphire regenerative amplifier (Spitfire, Spectra Physics) was used. This system delivers 120 fs pulses (9 nm full-width half-maximum –FWHM– in spectrum) at 1 kHz repetition rate with a central wavelength of 795 nm and up to 1 mJ of energy.

The input beam was split in two replicas. One replica serving as reference to be compared with the experimental results was directed towards a high-resolution multi-wave shearing interferometer (SID4-HR, Phasics) [8]. This type of wavefront sensors are particularly suitable for this application since they are achromatic and provide a high-dynamic range. The other replica entered the measurement pathway for wavefront retrieval using the algorithm above reported. BBO crystals were used to frequency double the beam to be measured. All of them were cut for perfect phase matching at 795 nm working at normal incidence ( $\alpha_s = 29.4^\circ$ ). Thickness values ranged between 300 and 1000  $\mu\text{m}$ .



The pulse energy in all our measurements is carefully chosen (with the help of a half-wave plate and a linear polarizer) in order to keep the intensity at the BBO crystal around or below  $\sim 2 \text{ GW/cm}^2$ . Working around this value, the intensity of the fundamental is low enough to make reasonably good our theoretical treatment as discussed in the previous section, and at the same time we get enough SH signal for performing the measurements with a very low noise level.

With the crystal properly aligned, the SH signal was maximized for a non-aberrated beam. A band-pass filter (FGB37S, Thorlabs) was placed after the crystal in order to eliminate the non-converted fundamental wave. The SH beam emerging from the BBO crystal passed a 4f-telescope composed of two achromatic lenses (AC254-175-A, Thorlabs) with a focal length of 175 mm. This telescope conjugated the SH signal at the exit of the crystal with the detection plane. At this detection plane, a fiber coupler (4  $\mu\text{m}$  core, Thorlabs S630-HP) was mounted on a motorized linear actuator for accurate controlled movements. The choice of the fiber core and the motor resolution determined the maximum resolution achievable in the reconstruction procedure. In our case, the positioning precision of the actuator is less than 1  $\mu\text{m}$  what ensures a maximum resolution limited by the fiber core. The scanning direction was chosen to be along the x-axis (according to Fig. 2). The spectrum data (see Fig. 3a) were recorded with a high resolution spectrometer (Ocean Optics, HR4000).

Although a large pulse energy could increase the SH signal making easier the detection, it cannot be arbitrarily large because breakdown of the air could occur in the intermediate focus of the optical system. To avoid this effect, we kept the incident pulse energy in the 10  $\mu\text{J}$  level.

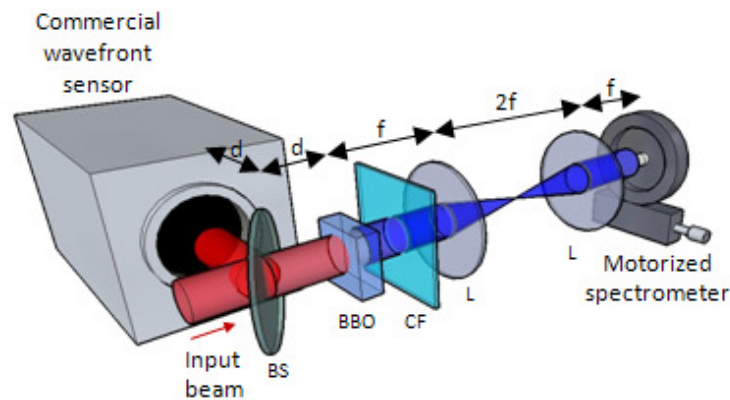


Fig. 4. Experimental setup. BS, beam-splitter; CF, band-pass filter; L, lenses; f, focal length of lenses; d, distance from BS to the BBO crystal and from BS to the wavefront sensor.

## 4. Results and discussion

### 4.1. Retrieved and measured wavefront aberration

The reliability and accuracy of the proposed phase retrieval method was tested on a femtosecond laser beam with different induced aberrations. As a first test, a convergent lens (400 mm focal length) was placed 354 mm away from the BBO crystal. The theoretical total aberration produced by this lens corresponded to a  $2.60\lambda$  (Peak-to-valley, PtV) phase distortion over a 0.86 mm pupil size. This aberrated beam passed a 500  $\mu\text{m}$  thick BBO crystal and reached the detection unit. At that plane the beam was scanned in 4  $\mu\text{m}$  steps (to be consistent with the fiber core size) to record the spectrum for each position along the x direction. This spectral map is shown in Fig. 5a. From this map and using the above described algorithm the corresponding wavefront was retrieved and is shown in Fig. 5c (blue markers). This result can be compared with the wavefront measured with the commercial sensor. This is shown with red symbols in Fig. 5c. Both of them were fit to a second order polynomial

(dashed lines in Fig. 5c), what allowed to calculate the Zernike coefficients. Values of  $2.53\lambda$  and  $2.58\lambda$  for defocus, and  $0.28\lambda$  and  $0.34\lambda$  of astigmatism (at  $0^\circ$ ) were obtained from the retrieval algorithm and the commercial sensor respectively.

Moreover, the coefficient of determination  $R^2$  was also computed. This is defined as:

$$R^2 = 1 - \frac{\sum_{i=1}^N (\psi_i - \phi_i)^2}{\sum_{i=1}^N (\psi_i - \bar{\psi})^2} \quad (7)$$

where  $\psi_i$  denotes the experimental wavefront values computed from the retrieval method,  $\phi_i$  those measured with the commercial sensor,  $\bar{\psi}$  the average and  $N$  is the number of steps made by the motor. For this measurement  $R^2$  was 0.994 what indicates a very good agreement between both calculations of the wavefront.

To validate the proposed method, a mathematical model of the wavefront sensor was also developed. This includes the reconstruction algorithm and simulates the whole process of the phase measurement. In this model, the phase distribution and the intensity profile recorded by the commercial sensor, as well as the spectrum of the fundamental beam are used as input data to simulate the spectral map according to the Eq. (1). The simulated trace is then introduced in the proposed algorithm for the phase retrieval. This allows to compare with the experimental results and to analyze the dependence with different parameters (see Figs. 5b and 5d).

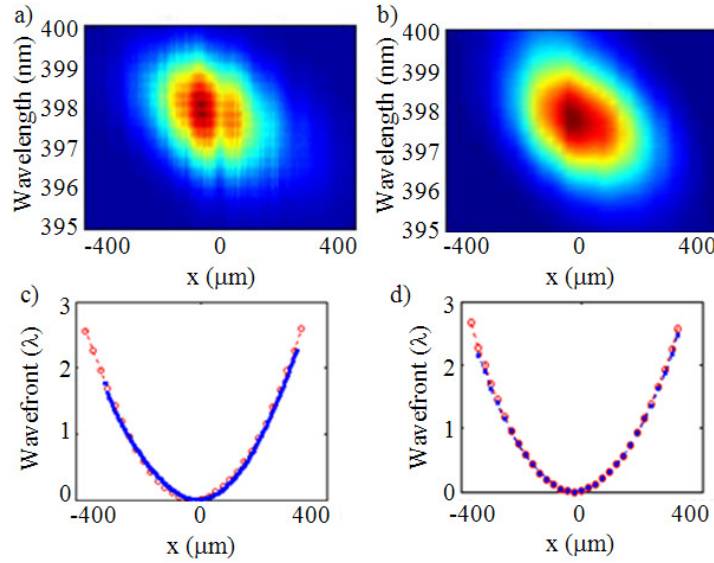


Fig. 5. Phase retrieval for an aberrated convergent beam (see details in the text). (a) Measured spectral map. (b) Simulated spectral map. Both, experimental and simulated spectral maps, are normalized. (c) Wavefront retrieved from (a) with the proposed algorithm (blue line). For comparison, we show the wavefront measured with the commercial sensor (red open dots). (d) Wavefront retrieved from (b) with the proposed algorithm (blue line) and wavefront measured with the commercial sensor (red open dots, same as in (c)).

Using the same conditions as in the experiment, the results for the simulated wavefront retrieval (Fig. 5b) were:  $2.50\lambda$  for defocus and  $0.32\lambda$  for  $0^\circ$  astigmatism. These values show how close the experimental results are from those obtained with the wavefront retrieval algorithm: 3.2% and 6.5% for defocus and astigmatism respectively. Two error sources could explain this deviation: (1) since the intensity drops at the edges of the beam the signal-to-noise ratio might decrease in all the spectral measurements; and (2) the phase matching



retrieval was done under the assumption of  $n_e(\lambda, \theta) \approx n_o(\lambda_c)$  in Eq. (2). This approximation might not be appropriate for wavelengths far from the central one and angles very different from the perfect phase matching condition.

#### 4.2. Effects of the non-linear crystal thickness

The influence of the non-linear crystal thickness on the wavefront retrieval was also investigated. Three BBO crystals (300, 500 and 1000  $\mu\text{m}$  in thickness) were used. The incident beam was set to different amounts of defocus keeping the same beam size.

As an example, the measured spectral maps for 300 and 1000  $\mu\text{m}$  thick crystals for two different values of defocus are shown in Fig. 6. Two main effects become evident from the figure. On one hand, the thicker the crystal, the stronger is the spectral modulation of the maps due to the phase mismatch factor. On the other hand, a larger amount of defocus is associated with more tilted spectral maps, since a larger range of angles is involved.

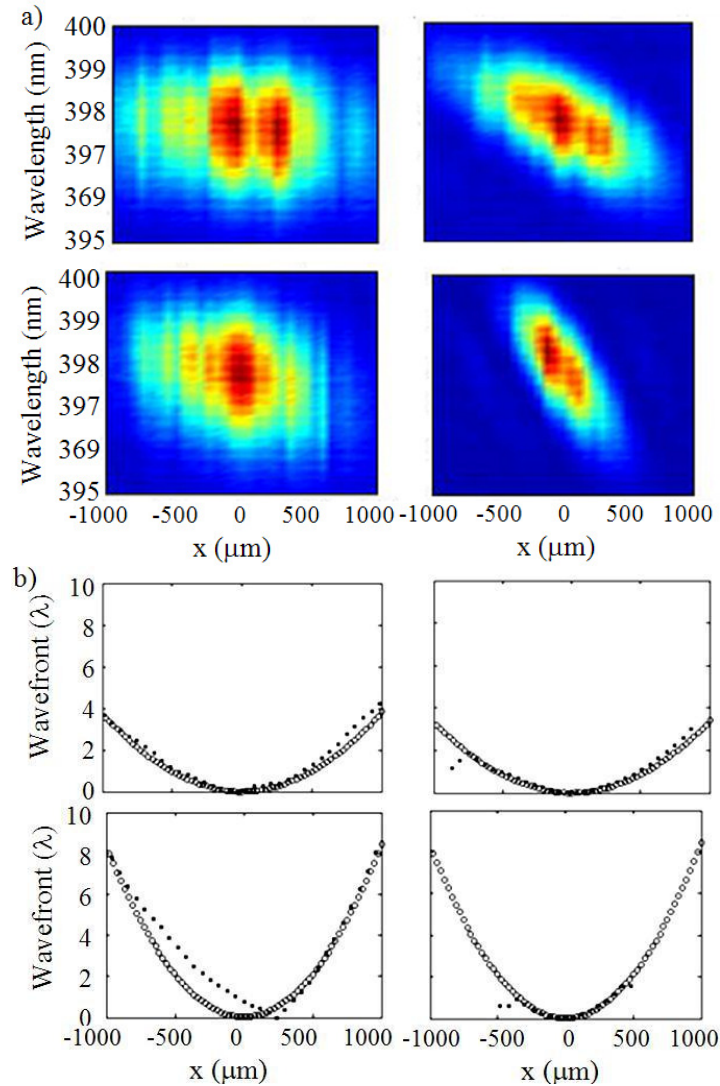


Fig. 6. (a) Spectral traces for 300  $\mu\text{m}$  (left panel) and 1000  $\mu\text{m}$  (right panel) thick BBO for  $0.95\lambda$  (upper panels) and  $1.84\lambda$  (lower panels) PtV defocus and a 1 mm pupil. All the traces are normalized. (b) Experimentally retrieved wavefront (black symbols) and wavefront measured with the commercial sensor (white symbols). The order is the same as in Fig. 6a.

From Eq. (1) it is possible to demonstrate that the generated SH has efficiency over 50% for a range of angles around the perfect phase matching angle satisfying:

$$\delta\theta = \frac{2.78\lambda}{\pi L} \frac{1}{\sin(2\theta_{PM})} \frac{1}{n_0(\lambda_{2\omega})} \left[ 1 - \frac{n_0^2(\lambda_{2\omega})}{n_z^2(\lambda_{2\omega})} \right]^{-1} \quad (8)$$

This value is usually termed as angular bandwidth [15] and it can be regarded as the range of propagation angles around the perfect phase matching value for which an efficient SH signal will be generated. The angular bandwidth constrains the order of the aberrations that can be successfully measured with the proposed technique: if the divergence between the wave vectors of a given wavefront exceeds this value, no appreciable SH signal will be produced and the accuracy of the retrieval will decrease. In Table 1 we show the comparison for different crystal thickness values for both, BBO and KDP crystals.

**Table 1. Angular acceptance of BBO and KDP for different crystal thickness**

	Crystal thickness		
	1000 $\mu\text{m}$	500 $\mu\text{m}$	300 $\mu\text{m}$
BBO	3.10 mrad	6.20 mrad	10.30 mrad
KDP	7.90 mrad	15.80 mrad	26.50 mrad

The crystal thickness is therefore a constrain parameter when measuring aberrations. First, according to Eq. (8) the thicker the crystal is, the lower the phase distortion that can be analyzed. Second, if the crystal is very thin, the reconstruction can be noisy, since the phase-matching curve becomes too broad and therefore more difficult to be retrieved. The optimal solution would be the choice of a crystal thickness with an angular bandwidth that exactly fits the aberration to measure. Obviously, this is meaningless in most of the cases provided that the aberration is unknown. Thus, the choice of a thin crystal will ensure at least the proper estimation of the aberration magnitude.

To take account of these effects, the coefficient of determination  $R^2$  according to Eq. (7), for the measurements performed in the different crystals was calculated. Results are summarized in Table 2. It can be seen that the largest value of  $R^2$  correspond to the crystal which angular acceptance best fits the PtV.

**Table 2. Experimental values for  $R^2$  with different crystal (BBO) thickness values and amounts of defocus (PtV, over a 1 mm pupil).**

PtV	Crystal thickness		
	300 $\mu\text{m}$	500 $\mu\text{m}$	1000 $\mu\text{m}$
1.84 $\lambda$	0.83	0.99	0.95
1.38 $\lambda$	0.92	0.98	0.95
0.95 $\lambda$	0.96	0.89	0.94

#### 4.3. Phase retrieval for wavefront with discontinuities

Finally, the robustness of the proposed technique was tested when applied to sharpen beam profiles. An example is shown in Fig. 7. In this case, the discontinuity was generated by partially blocking the laser beam with a knife-edge. The beam was focused by means of a 200 mm focal length lens. For the detection a 500  $\mu\text{m}$  thick BBO crystal was used. This was placed 110 mm away from the lens what corresponds to a 1.74 $\lambda$  PtV over a 1 mm pupil size. Since the phase is retrieved directly from the measurement and not from the derivatives, it is still possible to reconstruct the wavefront in spite of the discontinuities. Nevertheless, the retrieval gets worse with a  $R^2$  value of 0.92.

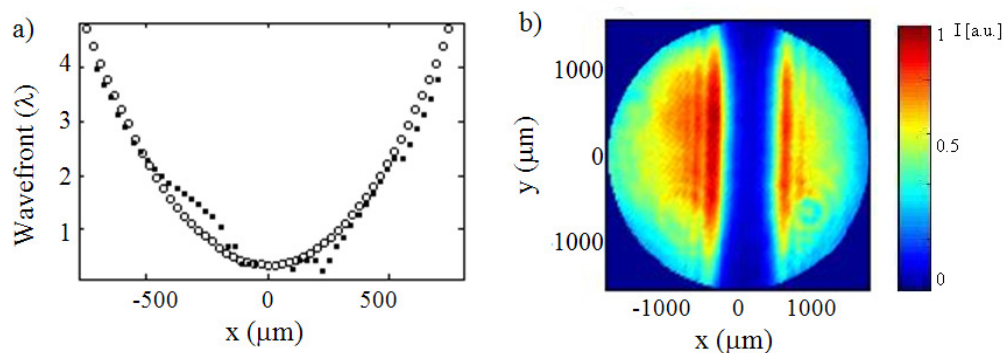


Fig. 7. (a) Retrieved wavefront for a beam with a discontinuity in the intensity profile (black squares) compared to the theoretically calculated wavefront (white dots). (b) Beam intensity profile recorded with a CCD camera.

## 5. Conclusions

We have developed and implemented a novel technique to retrieve the spatial phase of near transform-limited intense ultrashort pulses based on SHG in uniaxial non linear crystals. It requires the measurement of the spectrum of the generated SH pulse along one axis and applying a retrieval algorithm. The algorithm allows direct wavefront reconstruction with a deviation from the real phase that can reach less than 3%. Robust reconstruction for sharpen intensity patterns, such as discontinuities, have also been proved.

Since our experimental setup is based on a fiber spectrometer, by choosing a tiny core fiber and a high-precision linear stage we can get very high spatial resolution (down to 4 microns for the experiments here reported). This makes the technique suitable for measuring small beam sizes, conditions where other sensing methods do not always show very accurate results. For instance, in the Hartman-Shack sensor the size of each microlens (i.e. the pitch) imposes a limit to the spatial resolution of the wavefront reconstruction. Since each lens acts as a spatial integrator details smaller than its size cannot be captured. A limited spatial resolution would produce a smoother wavefront aberration, what might lead to an overestimation of the image quality of the system [23]. To our knowledge, the smaller commercially available pitch is 30 μm.

Moreover, since a spectrometer is included in our experimental setup, the presented procedure allows the measurement of the wavefront for the different spectral components of the incident beam. On the opposite, the spectral characterization of a broadband laser beam in terms of wavefront [6] with a Hartman-Shack sensor requires a set of narrow-band interference filters (as many as “wavelength slices” you want to measure). This advantage has not been explored in this work since with the current experimental conditions no dependence between the wavefront and the wavelength was found. However, this is particularly interesting for femtosecond pulses because chromatic aberration can be an issue, for example when using diffractive optics [24–26] or in the case of ultrahigh power lasers [27].

An important drawback is related to the choice of the crystal thickness, as it has been discussed. Thick crystals impose a limit to the range of aberrations to be measured. On the opposite, the thinner the crystal is, the larger the wavefront aberration that can be measured. However, the spectral maps will be noisier.

One of the disadvantages of the system with the present configuration is the time it takes to perform the measurements. This time depends on the resolution (i.e., number of steps performed by the motor) and the exposure time of the spectrometer. It could be reduced to a great extent if instead of a fiber mounted in a motorized stage, a slit-based imaging spectrograph were used, since in such case the scanning would be replaced by a single shot measurement.

Additionally, there are some issues one has to be very careful about. First, for the crystal thicknesses we are using (around 1 mm), the intensity must be kept under  $10 \text{ GW/cm}^2$  in order to avoid high-order nonlinear effects in the crystal (SPM, XPM...). Second, the technique cannot be applied in the case of strongly focusing beams, since non-collinear processes can become significant in the SHG process. Finally, a good alignment of the system is crucial to obtain a correct result. As in any imaging system, it is necessary to ensure that the object and image planes are perfectly conjugated. Furthermore in this case, the alignment of the crystal is very important for a right result.

As a final point, even though the method has been applied to the retrieval of the phase in one axis (that is enough for defocus aberration), the procedure shown here is general and can be implemented in 2D. In this case, the use of a slit-based imaging spectrograph could allow following an analogous procedure to that described in this work. The 1D wavefront retrieval demonstrated here might be very useful in beams providing cylindrical symmetry and in the analysis and optimization of telescopic systems and collimation devices.

### **Acknowledgments**

This research was funded by the Spanish Ministerio de Ciencia e Innovación (MICINN), through Consolider Program SAUUL CSD2007-00013 and research project FIS2009-09522, the Junta de Castilla y León through the Program for Groups of Excellence (GR27) and the EC's Seventh Framework Programme (LASERLAB-EUROPE, grant agreement n° 228334). Support from the Centro de Láseres Pulsados (CLPU) is also acknowledged. R. Borrego Varillas and C. Romero thank the MICINN for funding within the FPU and FPI programs respectively (grants no. AP2007-00202 and BES-2007-17415).